Efficient methods for solving the Stokes problem with slip boundary conditions

Radek Kučera, Jaroslav Haslinger, Václav Šátek, Marta Jarošová

VŠB-TU Ostrava, 17. listopadu 15/2172, 708 33 Ostrava-Poruba, CZ

Abstract

The paper deals with the Stokes flow with the threshold slip boundary conditions. A finite element approximation of the problem leads to the minimization of a non-differentiable energy functional subject to two linear equality constraints: the impermeability condition on the slip part of the boundary and the incompressibility of the fluid. Eliminating the velocity components, one gets the smooth dual functional in terms of three Lagrange multipliers. The first Lagrange multiplier regularizes the problem. Its components are subject to simple bounds. The other two Lagrange multipliers treat the impermeability and the incompressibility conditions. The last Lagrange multiplier represents the pressure in the whole domain. The solution to the dual problem is computed by an active set strategy and a path-following variant of the interior-point method. Numerical experiments illustrate computational efficiency.

Keywords: Stokes problem, slip boundary condition, active-set algorithm, interior-point method

1. Introduction

Observing a fluid flow along a solid impermeable wall, one can observe in some applications a non-zero tangential velocity of the fluid that may depend on a material of the wall or its shape. Such behaviour of the fluid is usually simulated by slip boundary conditions used for modelling the blood flow, the

Email address: radek.kucera@vsb.cz, hasling@karlin.mff.cuni.cz, vaclav.satek@vsb.cz (corresponding author), marta.jarosova@vsb.cz (Radek Kučera, Jaroslav Haslinger, Václav Šátek, Marta Jarošová)

metal forming processes, the polymer flow, or the hydrodynamics problems; see [15, 2] and references therein. Conditions of this type are used also in contact problems of solid mechanics, where they describe friction laws on common interfaces [9, 1]. Our paper deals with the slip boundary condition analogous to the Tresca friction law. To illustrate difficulties and still to keeping the ideas as clear as possible, we consider the Stokes problem in a planar domain Ω. The existence and uniqueness analysis of a weak solution of the problem is given in [2]. Some numerical results computed by the augmented Lagrangian method are reported in [7]. The aim of this paper is to extend optimization algorithms, which are highly efficient for contact problems to the Stokes problem with the slip boundary condition of the Tresca type.

The paper is organized as follows. In Section 2 we introduce equations describing the problem and present its weak formulation. Section 3 deals with the algebraic problem arising from the finite element approximation. Its dual formulation, i.e. the formulation in terms of the Lagrange multipliers, is derived. In Section 4, two algorithms for solving the dual problem are introduced: the algorithm based on the active set strategy [5, 3, 11] and the path-following variant of the interior-point method [16, 12]. Finally, Section 5 reports results of our numerical experiments computed by the P1-bubble/P1 and P2/P1 elements.

The symbol $\|\cdot\|$ stands for the Euclidean norm of vectors and the same symbol is used for the associated norm of matrices. If $\mathbf{x} \in \mathbb{R}^m$ and $\mathcal{A} \subseteq \{1, \ldots, m\}$ is an index set, then $\mathbf{x}_\mathcal{A}$ denotes the subvector of $\mathbf{x}$ with the indices belonging to $\mathcal{A}$. If $\mathcal{A} = \emptyset$, then $\mathbf{x}_\mathcal{A} = 0$. Finally $\mathbf{0}$ and $\mathbf{I}$ stand for the zero and the identity matrix, respectively, whose order will be seen from the context.

2. Formulation

Let Ω be a bounded domain in $\mathbb{R}^2$ with a sufficiently smooth boundary $\partial\Omega$ that is split into three disjoint parts: $\partial\Omega = \overline{\gamma}_D \cup \overline{\gamma}_N \cup \overline{\gamma}_C$. We consider the model of a viscous incompressible Newtonian fluid modelled by the Stokes system with the Dirichlet and Neumann boundary conditions on γ_D and γ_N, respectively, and with the impermeability and the slip boundary conditions

prescribed on γ_C:

$$\left.\begin{array}{rcll} -\nu\Delta\mathbf{u}+\nabla\mathtt{p} &=& \mathbf{f} & \text{in } \Omega,\\ \nabla\cdot\mathbf{u} &=& 0 & \text{in } \Omega,\\ \mathbf{u} &=& \mathbf{u}_D & \text{on } \gamma_D,\\ \boldsymbol{\sigma} &=& \boldsymbol{\sigma}_N & \text{on } \gamma_N,\\ \mathtt{u}_n &=& 0 & \text{on } \gamma_C,\\ |\sigma_t| &\le& \mathtt{g} & \text{on } \gamma_C,\\ |\sigma_t(\mathbf{x})|<\mathtt{g}(\mathbf{x}) \;\Rightarrow\; \mathtt{u}_t(\mathbf{x}) &=& 0 & \mathbf{x}\in\gamma_C,\\ |\sigma_t(\mathbf{x})|=\mathtt{g}(\mathbf{x}) \;\Rightarrow\; \exists k:=k(\mathbf{x})\ge 0:\ \mathtt{u}_t(\mathbf{x}) &=& -k\sigma_t(\mathbf{x}) & \mathbf{x}\in\gamma_C, \end{array}\right\} \quad (1)$$

where

$$\boldsymbol{\sigma}=\nu\frac{\mathrm{d}\mathbf{u}}{\mathrm{d}\mathbf{n}}-\mathtt{p}\mathbf{n}.$$

Here, $\mathbf{u}=(\mathtt{u}_1,\mathtt{u}_2)$ is the flow velocity, $\mathtt{p}$ is the pressure, $\mathbf{f}=(\mathtt{f}_1,\mathtt{f}_2)$ represents forces acting on the fluid, $\nu>0$ is the kinematic viscosity, and $\mathbf{u}_D$, $\boldsymbol{\sigma}_N$ are given the Dirichlet and Neumann boundary data, respectively. Further $\mathbf{n}$, $\mathbf{t}$ is the unit outer normal and tangential vector to $\partial\Omega$, respectively, and $\mathtt{u}_n=\mathbf{u}\cdot\mathbf{n}$, $\mathtt{u}_t=\mathbf{u}\cdot\mathbf{t}$ is the normal, tangential components of $\mathbf{u}$ along γ_C, respectively. Finally $\sigma_t=\boldsymbol{\sigma}\cdot\mathbf{t}$ is the shear stress and $\mathtt{g}\ge 0$ is the slip bound function on γ_C. We will assume that $\gamma_D\neq\emptyset$ and $\gamma_C\neq\emptyset$. For the sake of simplicity we will suppose that $\mathbf{u}_D=\mathbf{0}$.

Next we present the weak velocity-pressure formulation of (1). To this end we introduce the following notation:

$$V(\Omega)=\{\mathbf{v}\in\left(H^1(\Omega)\right)^2:\ \mathbf{v}=\mathbf{0}\ \text{ on } \gamma_D,\ \mathtt{v}_n=0\ \text{ on } \gamma_C\}$$

and

$$a(\mathbf{v},\mathbf{w})=\nu\int_\Omega\nabla\mathbf{v}:\nabla\mathbf{w}\,d\mathbf{x},\quad b(\mathbf{v},\mathtt{q})=-\int_\Omega\mathtt{q}(\nabla\cdot\mathbf{v})\,d\mathbf{x},$$

$$l(\mathbf{v})=\int_\Omega\mathbf{f}\cdot\mathbf{v}\,d\mathbf{x}+\int_{\gamma_N}\boldsymbol{\sigma}_N\cdot\mathbf{v}\,ds,\quad j(\mathbf{v})=\int_{\gamma_C}\mathtt{g}|\mathtt{v}_t|\,ds,$$

where $\nabla\mathbf{v}:\nabla\mathbf{w}=\nabla\mathtt{v}_1\cdot\nabla\mathtt{w}_1+\nabla\mathtt{v}_2\cdot\nabla\mathtt{w}_2$, $\mathbf{v}=(\mathtt{v}_1,\mathtt{v}_2)$, $\mathbf{w}=(\mathtt{w}_1,\mathtt{w}_2)$.

The velocity-pressure formulation of (1) reads as follows:

$$\left.\begin{array}{l} \textit{Find } (\mathbf{u},\mathtt{p})\in V(\Omega)\times L^2(\Omega) \textit{ such that}\\ a(\mathbf{u},\mathbf{v}-\mathbf{u})+b(\mathbf{v}-\mathbf{u},\mathtt{p})+j(\mathbf{v})-j(\mathbf{u})\ge l(\mathbf{v}-\mathbf{u})\quad\forall\mathbf{v}\in V(\Omega),\\ b(\mathbf{u},\mathtt{q})=0\quad\forall\mathtt{q}\in L^2(\Omega). \end{array}\right\} \quad (2)$$

The following theorem guarantees the existence and uniqueness of a weak solution.

Theorem 1. [2, 6] *Let* $\mathbf{f} \in (L^2(\Omega))^2$, $\boldsymbol{\sigma}_N \in (L^2(\gamma_N))^2$, *and* $\mathtt{g} \in L^\infty(\gamma_C)$, $\mathtt{g} \geq 0$. *Then the first component* $\mathbf{u}$ *of (2) exists and is unique. If* $\gamma_N \neq \emptyset$, *then the pressure* $\mathtt{p}$ *is unique as well, otherwise is unique up to an additive constant.*

To discretize (2) we use mixed finite elements. Let V_h and W_h be finite element approximations of $V(\Omega)$ and $L^2(\Omega)$, respectively. We will suppose that the pair (V_h, W_h) satisfies the *inf-sup* condition [6]. The discretization of (2) reads as follows:

$$\left.\begin{aligned} &\textit{Find } (\mathbf{u}_h, \mathtt{p}_h) \in V_h \times W_h \textit{ such that} \\ &a(\mathbf{u}_h, \mathbf{v}_h - \mathbf{u}_h) + b(\mathbf{v}_h - \mathbf{u}_h, \mathtt{p}_h) + j(\mathbf{v}_h) - j(\mathbf{u}_h) \geq l(\mathbf{v}_h - \mathbf{u}_h) \quad \forall \mathbf{v}_h \in V_h, \\ &b(\mathbf{u}_h, \mathtt{q}_h) = 0 \quad \forall \mathtt{q}_h \in W_h. \end{aligned}\right\} \tag{3}$$

3. Algebraic problems

The finite element approximation (3) together with an appropriate formula approximating j leads to the following algebraic problem:

$$\left.\begin{aligned} &\textit{Find } (\mathbf{u}, \mathbf{p}) \in \mathbb{R}^{n_u} \times \mathbb{R}^{n_p} \textit{ such that} \\ &\mathbf{u}^\top \mathbf{A}(\mathbf{v} - \mathbf{u}) + (\mathbf{v} - \mathbf{u})^\top \mathbf{B}^\top \mathbf{p} + \mathbf{g}^\top(|\mathbf{T}\mathbf{v}| - |\mathbf{T}\mathbf{u}|) \geq \mathbf{l}^\top(\mathbf{v} - \mathbf{u}) \quad \forall \mathbf{v} \in \mathbb{R}^{n_u}, \\ &\mathbf{q}^\top \mathbf{B}\mathbf{u} = 0 \quad \forall \mathbf{q} \in \mathbb{R}^{n_p}, \\ &\mathbf{N}\mathbf{u} = \mathbf{0}, \end{aligned}\right\} \tag{4}$$

where $\mathbf{A} \in \mathbb{R}^{n_u \times n_u}$ is a symmetric and positive definite stiffness matrix, $\mathbf{B} \in \mathbb{R}^{n_p \times n_u}$, $\mathbf{T}, \mathbf{N} \in \mathbb{R}^{n_c \times n_u}$ are full row-rank matrices, $\mathbf{l} \in \mathbb{R}^{n_u}$, $\mathbf{g} \in \mathbb{R}^{n_c}_+$, and $|\mathbf{x}| = (|x_1|, \ldots, |x_{n_c}|)^\top$ for $\mathbf{x} \in \mathbb{R}^{n_c}$; n_p is the total number of the nodes of a triangulation contained in $\overline{\Omega}$, n_c is the number of the nodes lying on $\overline{\gamma}_C \backslash \overline{\gamma}_D$, and n_u is the dimension of the solution component representing the velocity $\mathbf{u}$.

It is easy to show that (4) is equivalent to:

$$\textit{Find } \mathbf{u} \in \mathbb{V} \textit{ such that } \mathcal{J}(\mathbf{u}) \leq \mathcal{J}(\mathbf{v}) \quad \forall \mathbf{v} \in \mathbb{V}, \tag{5}$$

where $\mathcal{J}(\mathbf{v}) = \frac{1}{2}\mathbf{v}^\top \mathbf{A}\mathbf{v} - \mathbf{v}^\top \mathbf{l} + \mathbf{g}^\top |\mathbf{T}\mathbf{v}|$ and $\mathbb{V} = \{\mathbf{v} \in \mathbb{R}^{n_u} : \ \mathbf{N}\mathbf{v} = \mathbf{0}, \ \mathbf{B}\mathbf{v} = \mathbf{0}\}$. To remove the discrete impermeability condition $\mathbf{N}\mathbf{v} = \mathbf{0}$ and to regularize the last non-differentiable frictional term in $\mathcal{J}$, we introduce two algebraic Lagrange multipliers $\boldsymbol{\lambda}_n$ and $\boldsymbol{\lambda}_t$, respectively, and define the Lagrangian $\mathcal{L} : \mathbb{R}^{n_u} \times \Lambda \mapsto \mathbb{R}$ by

$$\mathcal{L}(\mathbf{v}, \boldsymbol{\lambda}) = \frac{1}{2}\mathbf{v}^\top \mathbf{A}\mathbf{v} - \mathbf{v}^\top \mathbf{l} + \boldsymbol{\lambda}^\top \mathbf{C}\mathbf{v},$$

where $\Lambda = \{\boldsymbol{\lambda}_t \in \mathbb{R}^{n_c} : \ |\boldsymbol{\lambda}_t| \leq \mathbf{g}\} \times \mathbb{R}^{n_c+n_p}$, $\boldsymbol{\lambda} = (\boldsymbol{\lambda}_t^\top, \boldsymbol{\lambda}_n^\top, \mathbf{p}^\top)^\top \in \Lambda$, and $\mathbf{C} = (\mathbf{T}^\top, \mathbf{N}^\top, \mathbf{B}^\top)^\top$. The minimization problem (5) is equivalent to the following saddle-point formulation:

$$\textit{Find } (\mathbf{u}, \bar{\boldsymbol{\lambda}}) \in \mathbb{R}^{n_u} \times \Lambda \textit{ s.t. } \mathcal{L}(\mathbf{u}, \boldsymbol{\lambda}) \leq \mathcal{L}(\mathbf{u}, \bar{\boldsymbol{\lambda}}) \leq \mathcal{L}(\mathbf{v}, \bar{\boldsymbol{\lambda}}) \quad \forall (\mathbf{v}, \boldsymbol{\lambda}) \in \mathbb{R}^{n_u} \times \Lambda. \tag{6}$$

Eliminating the velocity component $\mathbf{u} = \mathbf{A}^{-1}(\mathbf{l} - \mathbf{C}^\top \bar{\boldsymbol{\lambda}})$, we get the dual problem in terms of $\boldsymbol{\lambda}$ only:

$$\textit{Find } \bar{\boldsymbol{\lambda}} \in \Lambda \textit{ such that } \mathcal{S}(\bar{\boldsymbol{\lambda}}) \leq \mathcal{S}(\boldsymbol{\lambda}) \quad \forall \boldsymbol{\lambda} \in \Lambda \tag{7}$$

with

$$\mathcal{S}(\boldsymbol{\lambda}) = \frac{1}{2}\boldsymbol{\lambda}^\top \mathbf{F}\boldsymbol{\lambda} - \boldsymbol{\lambda}^\top \mathbf{d},$$

where $\mathbf{F} = \mathbf{C}\mathbf{A}^{-1}\mathbf{C}^\top$ is symmetric, positive definite and $\mathbf{d} = \mathbf{C}\mathbf{A}^{-1}\mathbf{l}$.

Remark 1. When the P1-bubble/P1 elements are used, the bubble-components are eliminated on the element level [10]. This changes the function $\mathcal{S}$, since $\mathbf{F} = \mathbf{C}\mathbf{A}^{-1}\mathbf{C}^\top + \mathit{diag}(\mathbf{0}, \mathbf{0}, \mathbf{E})$ and $\mathbf{d} = \mathbf{C}\mathbf{A}^{-1}\mathbf{l} + (\mathbf{0}^\top, \mathbf{0}^\top, \mathbf{c}^\top)^\top$, where $\mathbf{E} \in \mathbb{R}^{n_p \times n_p}$ is symmetric, positive definite and $\mathbf{c} \in \mathbb{R}^{n_p}$. This modification is without any conceptual difficulty, as $\mathbf{F}$ remains still symmetric and positive definite.

4. Algorithms

In this section, we introduce main ideas of the used algorithms. They are highly efficient for solving contact problems of solid mechanics, in particular the algorithms based on the active set strategy and on the path-following variant of the interior-point method.

4.1. Active set algorithm

Let $\mathcal{N} = \{1, \dots, 2n_c + n_p\}$ be the set of all indices and $\mathcal{A}(\boldsymbol{\lambda}) \subseteq \mathcal{N}$ be its subset containing indices of all active constraints at $\boldsymbol{\lambda} \in \Lambda$, i.e.,

$$\mathcal{A}(\boldsymbol{\lambda}) = \{i \in \mathcal{N} : |\lambda_{t,i}| = g_i\}.$$

Let $\mathbf{r}(\boldsymbol{\lambda}) = \mathbf{F}\boldsymbol{\lambda} - \mathbf{d}$ denote the gradient of $\mathcal{S}$ at $\boldsymbol{\lambda} \in \mathbb{R}^{2n_c+n_p}$. The projection $\mathbf{P}_\Lambda$ onto Λ at $\boldsymbol{\lambda}$ is characterized by

$$\mathbf{P}_\Lambda(\boldsymbol{\lambda}) = \arg\min_{\boldsymbol{\mu}\in\Lambda} \|\boldsymbol{\mu} - \boldsymbol{\lambda}\|.$$

The *reduced gradient* of $\mathcal{S}$ at $\boldsymbol{\lambda} \in \Lambda$ for a fixed $\alpha > 0$ is defined by

$$\widetilde{\mathbf{r}}(\boldsymbol{\lambda}) = \frac{1}{\alpha}(\boldsymbol{\lambda} - \mathbf{P}_\Lambda(\boldsymbol{\lambda} - \alpha\mathbf{r}(\boldsymbol{\lambda}))).$$

Note that the reduced gradient characterizes the optimality criterion to (7), i.e., $\bar{\boldsymbol{\lambda}}$ solves (7) iff $\widetilde{\mathbf{r}}(\bar{\boldsymbol{\lambda}}) = \mathbf{0}$. Moreover, if $\boldsymbol{\lambda} \neq \bar{\boldsymbol{\lambda}}$ and $\alpha > 0$ is sufficiently small, then the negative reduced gradient $-\widetilde{\mathbf{r}}(\boldsymbol{\lambda})$ is a descent direction at $\boldsymbol{\lambda} \in \Lambda$.

We combine the following steps to generate a sequence $\{\boldsymbol{\lambda}^{(k)}\}$ that approximates the solution $\bar{\boldsymbol{\lambda}}$ to (7):

(i) the *expansion* and *proportioning* steps $\boldsymbol{\lambda}^{(k+1)} = \boldsymbol{\lambda}^{(k)} - \alpha\widetilde{\mathbf{r}}(\boldsymbol{\lambda}^{(k)})$;

(ii) the *conjugate gradient* step $\boldsymbol{\lambda}^{(k+1)} = \boldsymbol{\lambda}^{(k)} - \alpha_{cg}^{(k)}\mathbf{p}^{(k)}$, where the step-length $\alpha_{cg}^{(k)}$ and the conjugate gradient directions $\mathbf{p}^{(k)}$ are computed recurrently [8]; the recurrence starts from $\boldsymbol{\lambda}^{(s)}$ generated by the last expansion or the proportioning step and does not change the active set, i.e., $\mathcal{A}(\boldsymbol{\lambda}^{(k+1)}) = \mathcal{A}(\boldsymbol{\lambda}^{(k)})$.

Although the expansion and proportioning steps are given by the same formula, their meaning is different. While the expansion step may preferably add indices to the current active set, the proportioning step may remove them. The conjugate gradient steps are used to carry out efficiently the minimization of $\mathcal{S}$ on the face $W(\boldsymbol{\lambda}^{(s)}) = \{\boldsymbol{\lambda} \in \Lambda : \ \boldsymbol{\lambda}_\mathcal{A} = \boldsymbol{\lambda}_\mathcal{A}^{(s)}, \mathcal{A} := \mathcal{A}(\boldsymbol{\lambda}^{(s)})\}$. Moreover, a constant $\Gamma > 0$ in the *proportioning criterion*

$$\widetilde{\mathbf{r}}_\mathcal{A}(\boldsymbol{\lambda}^{(k)})^\top \mathbf{r}_\mathcal{A}(\boldsymbol{\lambda}^{(k)}) \leq \Gamma\, \widetilde{\mathbf{r}}_{\mathcal{N}\setminus\mathcal{A}}(\boldsymbol{\lambda}^{(k)})^\top \mathbf{r}_{\mathcal{N}\setminus\mathcal{A}}(\boldsymbol{\lambda}^{(k)}) \tag{8}$$

is introduced in order to decide which of the steps will be performed.

ALGORITHM AS: Let $\boldsymbol{\lambda}^{(0)} \in \Lambda$, $\Gamma > 0$, $\alpha \in (0, 2\|\mathbf{F}\|^{-1})$, and $\varepsilon > 0$ be given. For $\boldsymbol{\lambda}^{(k)}$, $\boldsymbol{\lambda}^{(s)}$ known, $0 \leq s \leq k$, where $\boldsymbol{\lambda}^{(s)}$ is computed by the last expansion or proportioning step, choose $\boldsymbol{\lambda}^{(k+1)}$ by the following rules:

(i). If $\|\widetilde{\mathbf{r}}(\boldsymbol{\lambda}^{(k)})\| \leq \varepsilon$, return $\bar{\boldsymbol{\lambda}} = \boldsymbol{\lambda}^{(k)}$;

(ii). If $\boldsymbol{\lambda}^{(k)}$ fulfils (8), try to generate $\boldsymbol{\lambda}^{(k+1)}$ by the conjugate gradient step. If $\boldsymbol{\lambda}^{(k+1)} \in W(\boldsymbol{\lambda}^{(s)})$, accept it, otherwise generate $\boldsymbol{\lambda}^{(k+1)}$ by the expansion step;

(iii). If $\boldsymbol{\lambda}^{(k)}$ does not fulfil (8), generate $\boldsymbol{\lambda}^{(k+1)}$ by the proportioning step.

This algorithm is a slight modification of the ones studied in [5, 3, 11, 4]. In principle, the same analysis with the same convergence results can be established.

4.2. Path-following algorithm

Let the Lagrangian to (7) be defined by

$$L(\boldsymbol{\lambda}, \boldsymbol{\mu}) = \mathcal{S}(\boldsymbol{\lambda}) + \boldsymbol{\mu}_1^\top(-\boldsymbol{\lambda} - \mathbf{g}) + \boldsymbol{\mu}_2^\top(\boldsymbol{\lambda} - \mathbf{g}),$$

where $\boldsymbol{\mu} = (\boldsymbol{\mu}_1^\top, \boldsymbol{\mu}_2^\top)^\top \in \mathbb{R}^{2n_c}$ is the Lagrange multiplier associated with two-side constraint appearing in Λ. Let $\mathbf{z} := -\nabla_\mu L(\boldsymbol{\lambda}, \boldsymbol{\mu})$ be the new variable and introduce the function $\mathbf{G} : \mathbb{R}^{6n_c+n_p} \mapsto \mathbb{R}^{6n_c+n_p}$ by

$$\mathbf{G}(\mathbf{w}) := (\nabla_\lambda L(\boldsymbol{\lambda}, \boldsymbol{\mu})^\top, (\nabla_\mu L(\boldsymbol{\lambda}, \boldsymbol{\mu}) + \mathbf{z})^\top, \mathbf{e}^\top \mathbf{M}\mathbf{Z})^\top,$$

where $\mathbf{w} = (\boldsymbol{\lambda}^\top, \boldsymbol{\mu}^\top, \mathbf{z}^\top)^\top \in \mathbb{R}^{6n_c+n_p}$, $\mathbf{M} = diag(\boldsymbol{\mu})$, $\mathbf{Z} = diag(\mathbf{z})$, and $\mathbf{e} \in \mathbb{R}^{2n_c}$ is the vector whose all components are equal to 1. The solution $\bar{\boldsymbol{\lambda}}$ to (7) is the first component of the vector $\bar{\mathbf{w}} = (\bar{\boldsymbol{\lambda}}^\top, \bar{\boldsymbol{\mu}}^\top, \bar{\mathbf{z}}^\top)^\top$, which satisfies

$$\mathbf{G}(\mathbf{w}) = \mathbf{0},\ \boldsymbol{\mu} \geq \mathbf{0},\ \mathbf{z} \geq \mathbf{0}, \tag{9}$$

since (9) is equivalent to the Karush-Khun-Tucker conditions.

To derive the path-following algorithm, we replace (9) by the following perturbed problem:

$$\mathbf{G}(\mathbf{w}) = (\mathbf{0}^\top, \mathbf{0}^\top, \tau\mathbf{e}^\top)^\top,\ \boldsymbol{\mu} > 0,\ \mathbf{z} > \mathbf{0}, \tag{10}$$

where $\tau \in \mathbb{R}_+$. Solutions $\mathbf{w}^\tau$ to (10) define a curve $\mathcal{C}(\tau)$ in $\mathbb{R}^{6n_c+n_p}$ called the *central path*. This curve approaches $\bar{\mathbf{w}}$ when τ tends to zero. We combine the damped Newton method used for solving the equation in (10) with an appropriate change of τ which guarantees that the iterations belong to a neighbourhood $\mathcal{N}(c_1, c_2)$ of $\mathcal{C}(\tau)$ defined by

$$\begin{aligned}\mathcal{N}(c_1, c_2) \ = \ \{\mathbf{w} = (\boldsymbol{\lambda}^\top, \boldsymbol{\mu}^\top, \mathbf{z}^\top)^\top \in \mathbb{R}^{6n_c+n_p} :\ & \mu_i z_i \geq c_1\vartheta,\ i = 1, \ldots, 2n_c, \\ & \boldsymbol{\mu} \geq \mathbf{0},\ \mathbf{z} \geq \mathbf{0},\ \|\nabla_\lambda L(\boldsymbol{\lambda}, \boldsymbol{\mu})\| \leq c_2\vartheta,\ \|\nabla_\mu L(\boldsymbol{\lambda}, \boldsymbol{\mu}) + \mathbf{z}\| \leq c_2\vartheta\},\end{aligned}$$

where $c_1 \in (0,1]$, $c_2 \geq 0$, and $\vartheta := \vartheta(\mathbf{w}) = \boldsymbol{\mu}^\top \mathbf{z}/(2n_c)$. In the k-th iteration, we modify $\tau := \tau^{(k)}$ by the product of $\vartheta^{(k)} = \vartheta(\mathbf{w}^{(k)})$ with the centering parameter $c^{(k)}$ chosen as in [13]. The algorithm uses also the *Armijo-type condition* (12) ensuring that the sequence $\{\vartheta^{(k)}\}$ is monotonically decreasing. By $\mathbf{J}(\mathbf{w})$ in (11), we denote the Jacobi matrix of $\mathbf{G}$ at $\mathbf{w}$.

ALGORITHM PF: Given $c_1 \in (0,1]$, $c_2 \geq 1$, $0 < c_{\min} \leq c_{\max} \leq 1/2$, $\omega \in (0,1)$, and $\varepsilon \geq 0$. Let $\mathbf{w}^{(0)} \in \mathcal{N}(c_1, c_2)$ and set $k := 0$.

(i). Choose $c^{(k)} \in [c_{\min}, c_{\max}]$;

(ii). Solve

$$\mathbf{J}(\mathbf{w}^{(k)})\Delta\mathbf{w}^{(k+1)} = -\mathbf{G}(\mathbf{w}^{(k)}) + (\mathbf{0}^\top, \mathbf{0}^\top, c^{(k)}\vartheta^{(k)}\mathbf{e}^\top)^\top; \qquad (11)$$

(iii). Set $\mathbf{w}^{(k+1)} = \mathbf{w}^{(k)} + \alpha^{(k)}\Delta\mathbf{w}^{(k+1)}$ with the largest $\alpha^{(k)} \in (0,1]$ satisfying $\mathbf{w}^{(k+1)} \in \mathcal{N}(c_1, c_2)$ and

$$\vartheta^{(k+1)} \leq (1 - \alpha^{(k)}\omega(1 - c^{(k)}))\vartheta^{(k)}; \qquad (12)$$

(iv). Return $\bar{\mathbf{w}} = \mathbf{w}^{(k+1)}$, if $err^{(k)} := \|\mathbf{w}^{(k+1)} - \mathbf{w}^{(k)}\|/\|\mathbf{w}^{(k+1)}\| \leq \varepsilon$, else set $k := k + 1$ and go to step (i).

The bounds on the parameters mentioned in the initialization section follow from the convergence analysis presented in [12].

The computational efficiency depends on the way how the inner linear systems (11) are solved. The Jacobi matrix is non-symmetric and indefinite with the following block structure:

$$\mathbf{J}(\mathbf{w}^{(k)}) = \begin{pmatrix} \mathbf{F} & \mathbf{J}_{12} & \mathbf{0} \\ \mathbf{J}_{12}^\top & \mathbf{0} & \mathbf{I} \\ \mathbf{0} & \mathbf{Z} & \mathbf{M} \end{pmatrix}, \quad \mathbf{J}_{12} = \begin{pmatrix} -\mathbf{I} & \mathbf{I} \\ \mathbf{0} & \mathbf{0} \end{pmatrix}.$$

Eliminating the 2nd and 3rd unknown of $\Delta\mathbf{w}^{(k+1)}$, we get the reduced linear system for $\Delta\boldsymbol{\lambda}^{(k+1)}$ with the Schur complement

$$\mathbf{J}_{SC} = \mathbf{F} + \mathbf{M}_1\mathbf{Z}_1^{-1} + \mathbf{M}_2\mathbf{Z}_2^{-1},$$

where $\mathbf{Z} = diag(\mathbf{Z}_1, \mathbf{Z}_2)$ and $\mathbf{M} = diag(\mathbf{M}_1, \mathbf{M}_2)$. As $\boldsymbol{\mu}^{(k)} > \mathbf{0}$, $\mathbf{z}^{(k)} > \mathbf{0}$, the matrix $\mathbf{J}_{SC}$ is symmetric, positive definite and the reduced linear system

can be solved by the conjugate gradient method. In order to guarantee its convergence, we use the preconditioner:

$$\mathbf{P}_{SC} = \mathbf{D} + \mathbf{M}_1\mathbf{Z}_1^{-1} + \mathbf{M}_2\mathbf{Z}_2^{-1},$$

where $\mathbf{D} = diag(\mathbf{F})$. The eigenvalues of the preconditioned matrix $\mathbf{P}_{SC}^{-1}\mathbf{J}_{SC}$ belong to an interval which does not depend on the iteration and the spectral condition number is bounded by (see [12]):

$$\kappa(\mathbf{P}_{SC}^{-1}\mathbf{J}_{SC}) \leq \kappa(\mathbf{D})\kappa(\mathbf{F}).$$

In computations, we approximate $\mathbf{D}$ so that $\mathbf{A}^{-1}$ in $\mathbf{F}$ is replaced by $diag(\mathbf{A})^{-1}$.

The conjugate gradient method used in the k-th step of ALGORITHM PF is initialized and terminated adaptively. The initial iteration is taken as the computed result in the previous iteration and the (inner) iterations are terminated, if the relative residuum is less than the stopping tolerance given by

$$tol^{(k)} = \min\{r_{tol} \times err^{(k-1)}, c_{fact} \times tol^{(k-1)}\},$$

where $0 < r_{tol} < 1$, $0 < c_{fact} < 1$, $err^{(-1)} = 1$, and $tol^{(-1)} = r_{tol}/c_{fact}$.

5. Numerical experiments

The problem is approximated by the P1-bubble/P1 [10] and P2/P1 [6] elements on triangular meshes. The frictional term $j(\mathbf{v}_h)$ in (3) is evaluated using the numerical integration:

$$j(\mathbf{v}_h) = \int_{\gamma_C} \mathrm{g}|\mathrm{v}_{ht}|\, ds \approx \sum_{\mathbf{x}_i \in N_{cont}} \omega_i \mathrm{g}(\mathbf{x}_i)|\mathrm{v}_{ht}(\mathbf{x}_i)| =: \mathbf{g}^\top|\mathbf{T}\mathbf{v}|, \qquad (13)$$

where N_{cont} is the set of integration points and ω_i are weights of a quadrature formula. Below we use N_{cont} given by triangle vertices (nodes) lying on $\overline{\gamma}_C \backslash \overline{\gamma}_D$. In general, γ_C is approximated by a polygon and ω_i are chosen so that (13) represents the trapezoidal rule over this polygon.

All codes are implemented in Matlab 2013b. The computations were performed by ANSELM supercomputer at IT4I VŠB-TU Ostrava. We use ALGORITHM AS with $\varepsilon = tol_{AS} \times \|\mathbf{d}\|$, $\Gamma = 1$, $\alpha = 1.9\|\mathbf{F}\|$ and ALGORITHM PF with $c_1 = 0.001$, $c_2 = 10^9$, $c_{\min} = 10^{-12}$, $c_{\max} = 0.5$, $\omega = 0.01$, $\varepsilon = tol_{PF}$, $r_{tol} = 0.5$, $c_{fact} = 0.9$. The values of these parameters seem to be optimal, as follows from the results in [5, 3, 11] or from the tests in [12]. The

terminating tolerances tol_{AS} and tol_{PF} will be taken differently in order to get the comparable relative residua on the level 10^{-5} from both ALGORITHM AS and ALGORITHM PF, respectively. The symbol ">number" used in tables below stands for situations, when the terminating tolerance is not achieved for the default maximum number of iterations.

Example 1 (square domain). Let $\Omega = (0,1)\times(0,1)$, $\gamma_D = (0,1)\times\{1\}$, $\gamma_{N_{left}} = \{0\}\times(0,1)$, $\gamma_{N_{right}} = \{1\}\times(0,1)$, $\gamma_N = \gamma_{N_{left}} \cup \gamma_{N_{right}}$, and $\gamma_C = (0,1)\times\{0\}$. The data of problem (1) are defined as follows: $\mathbf{f} = -\nu\Delta\mathbf{u}_{exp} + \nabla \mathtt{p}_{exp}$, $\nu = 1$, $\mathbf{u}_D = \mathbf{0}$, $\boldsymbol{\sigma}_N = \boldsymbol{\sigma}_{exp|_{\gamma_N}}$, and $\mathtt{g} = 10$, where $\mathbf{u}_{exp}(x,y) = (-\cos(2\pi x)\sin(2\pi y) + \sin(2\pi y), \sin(2\pi x)\cos(2\pi y) - \sin(2\pi x))$ and $\mathtt{p}_{exp}(x,y) = 2\pi(\cos(2\pi y) - \cos(2\pi x))$. Note that $\mathbf{u}_{exp}$ and $\mathtt{p}_{exp}$ do not solve (1). The finite element mesh, the velocity, and the pressure field are drawn in Fig. 1.

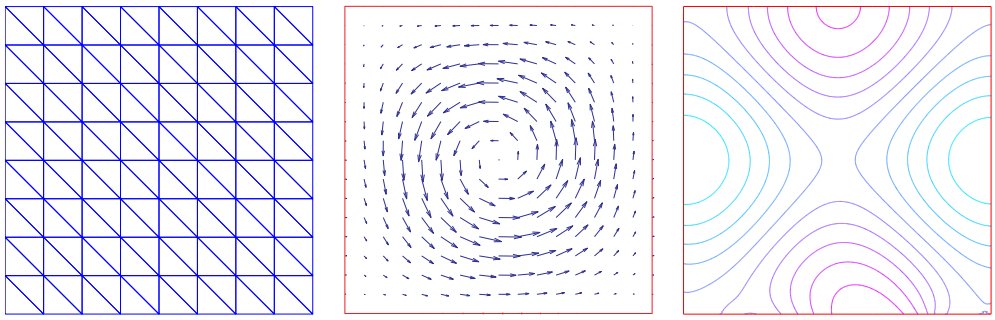

Figure 1: Mesh (left), velocity field (middle), isobars (right).

The convergence rate of the finite element approximation is evaluated in Tab. 1 and 2 as follows:

$$\begin{aligned} Err_1(h) &= \|\mathbf{u}_h - \mathbf{u}_{ref}\|_{L^2(\Omega)}, \\ Err_2(h) &= \|\mathbf{u}_h - \mathbf{u}_{ref}\|_{H^1(\Omega)} + \|\mathtt{p}_h - \mathtt{p}_{ref}\|_{L^2(\Omega)}, \\ Rate_j(h) &= \log_2(Err_j(h)/Err_j(h/2)), \quad j = 1,2. \end{aligned}$$

Here, h denotes the length of the largest edge, $\mathbf{u}_h$, $\mathtt{p}_h$ is the corresponding finite element solution, and $\mathbf{u}_{ref}$, $\mathtt{p}_{ref}$ is the reference solution computed on the finest mesh with $h = 1/512$. Figure 2 left and middle illustrate the distribution of the shear stress along γ_C for the P1-bubble/P1 and P2/P1 elements, respectively. If the set N_{cont} for the P2/P1 elements contains also

midpoints of the triangular edges lying on γ_C (that are used for representing the velocity), then the approximation of σ_t oscillates; see Fig. 2 right. This fact may be due to the non-satisfaction of the *inf-sup* stability condition by the Lagrange multipliers in this case. Our choice of N_{cont} can be viewed as a kind of under-integration of the frictional term (13) resulting in a lower convergence rate as seen from Tab. 2. The slip boundary condition is satisfied in a weak sense.

h	$Err_1(h)$	$Rate_1(h)$	$Err_2(h)$	$Rate_2(h)$
1/16	5.424×10^{-2}	–	5.624×10^{-1}	–
1/32	1.421×10^{-2}	1.93	1.732×10^{-1}	1.70
1/64	3.505×10^{-3}	2.02	5.422×10^{-2}	1.68
1/128	8.381×10^{-4}	2.09	1.778×10^{-2}	1.61
1/256	1.668×10^{-4}	2.33	6.541×10^{-3}	1.44

Table 1: Convergence rate for P1-bubble/P1.

h	$Err_1(h)$	$Rate_1(h)$	$Err_2(h)$	$Rate_2(h)$
1/8	1.638×10^{-1}	–	1.895×10^{0}	–
1/16	8.425×10^{-2}	0.96	1.317×10^{0}	0.52
1/32	4.290×10^{-2}	0.97	9.237×10^{-1}	0.51
1/64	2.161×10^{-2}	0.98	6.488×10^{-1}	0.51
1/128	1.085×10^{-2}	0.99	4.566×10^{-1}	0.51

Table 2: Convergence rate for P2/P1.

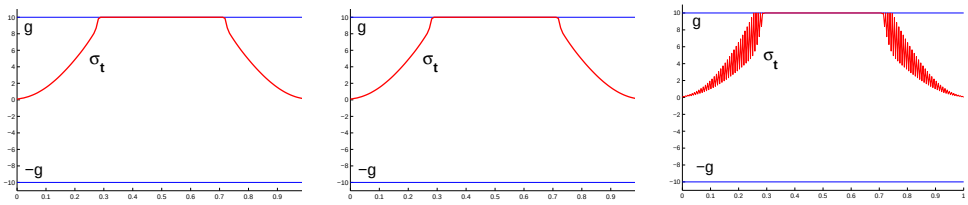

Figure 2: P1-bubble/P1 (left), P2/P1 stable (middle), P2/P1 unstable (right).

Example 2 (curved slip boundary). The previous example is modified by changing the slip part of the boundary: $\gamma_C = \{(x, -0.1\sin(2\pi x)) : x \in (0,1)\}$; see Fig. 3. On γ_C we prescribe different values of g in order to illustrate friction effects that are seen in Fig. 4. In Tab. 3 and 4 we show the number of matrix-vector multiplications by $\mathbf{F}$ for ALGORITHM AS with $tol_{AS} = 10^{-5}$ and ALGORITHM PF with $tol_{PF} = 10^{-3}$. Note that the dual problem (7) contains only n_c components (of $\boldsymbol{\lambda}_t$) subject to constraints, while remaining $n_c + n_p$ components (of $\boldsymbol{\lambda}_n$ and $\mathbf{p}$) are unconstrained. This fact influences considerably computational complexity of the algorithms. Since $n_p \gg n_c$ for finer meshes, ALGORITHM PF is more efficient than ALGORITHM AS (for non-trivial situation with $\mathsf{g} = 10$).

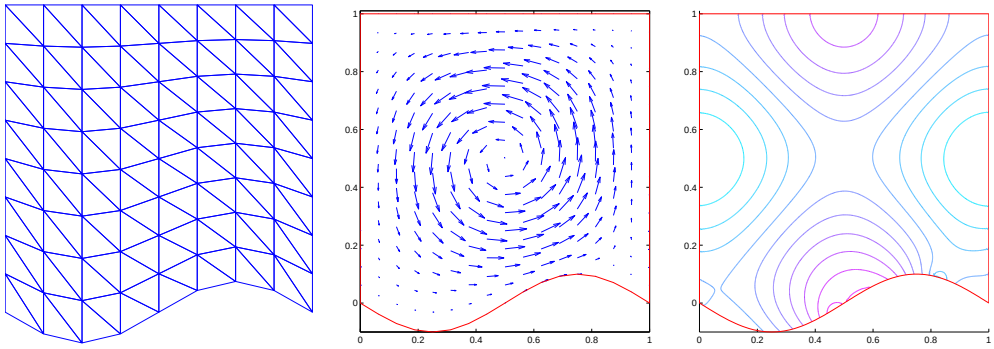

Figure 3: Mesh (left), velocity field (middle), isobars (right).

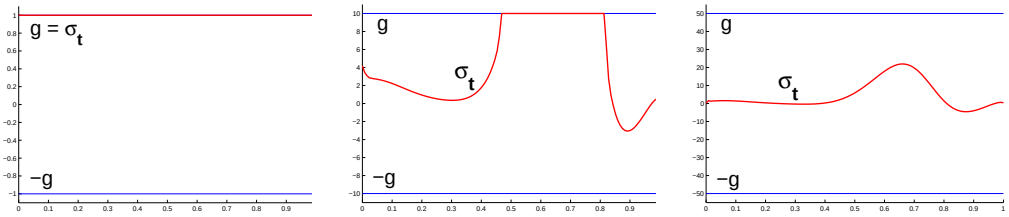

Figure 4: $\mathsf{g} = 1$ (left), $\mathsf{g} = 10$ (middle), $\mathsf{g} = 50$ (right).

slip bound	g = 1		g = 10		g = 50	
$n_u/n_p/n_c$	AS	PF	AS	PF	AS	PF
544/289/17	**91**	**115**	**250**	**127**	**125**	**157**
2112/1089/33	**111**	**117**	**1094**	**178**	**151**	**153**
8320/4225/65	**151**	**113**	**4993**	**194**	**205**	**216**
33024/16641/129	**123**	**170**	>5000	**259**	**676**	**180**
131584/66049/257	**184**	**173**	>5000	**252**	**2090**	**319**

Table 3: P1-bubble/P1 elements: multiplications by **F** in ALG. AS and PF.

slip bound	g = 1		g = 10		g = 50	
$n_u/n_p/n_c$	AS	PF	AS	PF	AS	PF
544/81/9	**58**	**80**	**128**	**98**	**67**	**93**
2112/289/17	**78**	**97**	**271**	**110**	**85**	**99**
8320/1089/33	**82**	**96**	**870**	**119**	**100**	**87**
33024/4225/65	**102**	**105**	**3153**	**107**	**150**	**123**
131584/16641/129	**111**	**116**	>5000	**187**	**273**	**114**

Table 4: P2/P1 elements: multiplications by **F** in ALG. AS and PF.

Example 3 (domain with a circular inclusion). Let $\Omega = (-0.2, 2)\times(-0.2, 0.2)\setminus \overline{\mathcal{C}}$, where $\mathcal{C}$ is the circle with center at the origin and radius $r = 0.05$. The decomposition of the boundary $\partial\Omega$ is as follows: $\gamma_D = \gamma_{D,1} \cup \gamma_{D,2} \cup \gamma_{D,3}$, $\gamma_{D,1} = (-0.2, 2) \times \{-0.2\}$, $\gamma_{D,2} = (-0.2, 2) \times \{0.2\}$, $\gamma_{D,3} = \{-0.2\} \times (-0.2, 0.2)$, $\gamma_N = \{2\} \times (-0.2, 0.2)$, and $\gamma_C = \partial\mathcal{C}$. The problem (1) is solved for $\mathbf{f} = \mathbf{0}$, $\nu = 1$, $\mathbf{u}_{D|_{\gamma_{D,1}\cup\gamma_{D,2}}} = \mathbf{0}$, $\mathbf{u}_{D|_{\gamma_{D,3}}} = 7.5(0.04 - y^2, 0)$ with $y \in (-0.2, 0.2)$, and $\boldsymbol{\sigma}_N = \mathbf{0}$. The non-uniform meshes on Ω are assembled by the mesh generator available at [14]. The solution with $\mathsf{g} = 10$ computed by the P1-bubble/P1 elements is shown in Fig. 5. This solution is partially slipping and partially sticking on γ_C; see Fig. 6. The solution computed for $\mathsf{g} = 30$ is solely sticking; see Fig. 7. The third situation (i.e., solely slipping solution) does not appear in this example for any g. In Tables 5 and 6 we show the number of matrix-vector multiplications by $\mathbf{F}$ for ALGORITHM AS with $tol_{AS} = 10^{-5}$ and ALGORITHM PF with $tol_{PF} = 10^{-4}$ and in parenthesis the CPU time.

slip bound	$\mathsf{g} = 10$		$\mathsf{g} = 30$	
$n_u/n_p/n_c$	AS	PF	AS	PF
862/526/30	**6867**(7.2)	**208**(0.6)	**682**(1.2)	**181**(0.2)
3566/1972/60	**22579**(118.6)	**283**(12.4)	**1060**(8.4)	**268**(1.2)
14494/7624/120	**130615**(4110.4)	**374**(12.4)	**1816**(59.2)	**389**(12.7)
58430/29968/240	>200000	**459**(135.4)	**3083**(849.1)	**454**(130.7)

Table 5: P1-bubble/P1 elements: multiplications by $\mathbf{F}$ in ALG. AS and PF (and CPU time in seconds).

slip bound	$\mathsf{g} = 10$		$\mathsf{g} = 30$	
$n_u/n_p/n_c$	AS	PF	AS	PF
3566/526/30	**3438**(407.1)	**190**(32.8)	**472**(58.5)	**151**(27.7)
14494/1972/60	>10000	**255**(568.2)	**748**(944.5)	**171**(398.5)
58430/7624/120	>10000	**293**(13723.7)	>10000	**266**(12327.9)

Table 6: P2/P1 elements: multiplications by $\mathbf{F}$ in ALG. AS and PF (and CPU time in seconds).

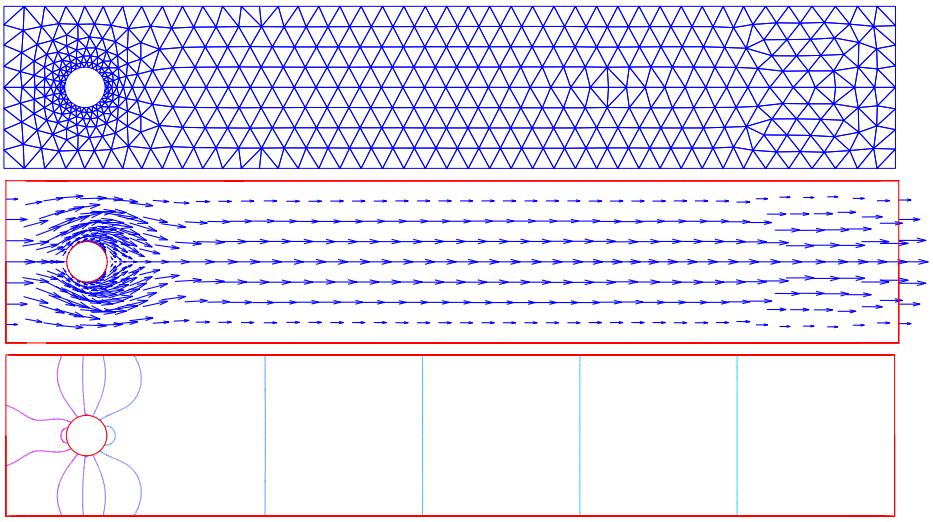

Figure 5: Mesh (upper), velocity field (middle), and isobars (bottom).

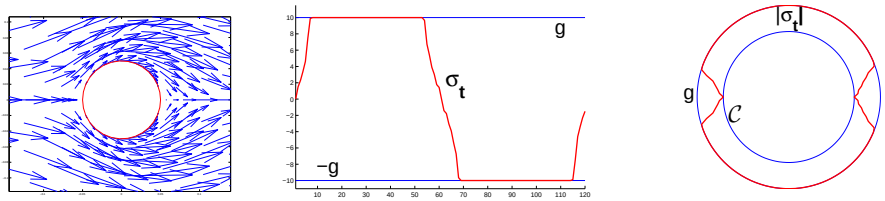

Figure 6: Zoom of the velocity field around the circle $\mathcal{C}$ (left); distribution of σ_t along the slip boundary for $\mathsf{g} = 10$ (middle and right).

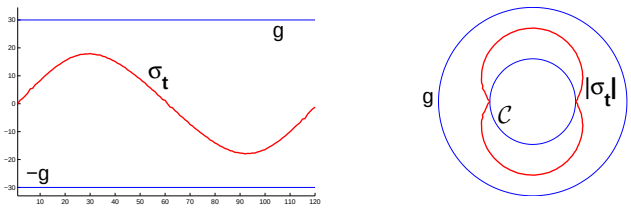

Figure 7: Distribution of σ_t along the slip boundary for $\mathsf{g} = 30$.

The character of our problem, i.e. small number (n_c) of constrained unknowns versus large number ($n_c + n_p = n_c + \mathcal{O}(n_c^2)$) of unconstrained ones, influences considerably efficiency of computations. ALGORITHM AS behaves as the restarted conjugate gradient method with many restarts and with some long sequences of continuous conjugate gradient loops between two restarts. Moreover, the unknowns corresponding to the active set are "dead" during one continuous conjugate gradient loop. On the other hand, all unknowns are "always living" in ALGORITHM PF. Therefore, this algorithm may be interpreted as one conjugate gradient loop with driven perturbations in its subsequences. This perturbations are less dramatic than the change of the active unknown to the inactive one or conversely. The convergence process of ALGORITHM PF is more balanced that leads to its high computational efficiency.

Acknowledgement

This work was supported by the European Development Fund in the IT4Innovations Centre of Excellence project CZ.1.05/1.1.00/02.0070 and by the project New creative teams in priorities of scientific research, reg. no. CZ.1.07/2.3.00/30.0055, supported by Operational Programme Education for Competitiveness and co-financed by the European Social Fund and the state budget of the Czech Republic. The last author was partially supported by the Grant Agency of the Czech Republic (GACR 13-30657P).

References

[1] M. Anitescu, F. A. Potra, Formulating dynamic multi-rigid-body contact problems with friction as solvable linear complementarity problems, Nonlinear Dynamics 14 (1997) 231–247.

[2] M. Ayad, L. Baffico, M. K. Gdoura, T. Sassi, Error estimates for stokes problem with tresca friction conditions, ESAIM: Mathematical Modelling and Numerical Analysis (accepted 2014).

[3] Z. Dostál, Optimal Quadratic Programming Algorithms: with Applications to Variational Inequalities, SOIA 23, Springer US, New York, 2009.

[4] Z. Dostál, T. Kozubek, An optimal algorithm and superrelaxation for minimization of a quadratic function subject to separable convex constraints with applications, Mathematical Programming 135 (2012) 195–220.

[5] Z. Dostál, J. Schöberl, Minimizing quadratic functions subject to bound constraints with the rate of convergence and finite termination, Computational Optimization and Applications 30 (2005) 23–44.

[6] H. C. Elman, D. J. Silvester, A. J. Wathen, Finite Elements and Fast Iterative Solvers with Applications in Incompressible Fluid Dynamics, Oxford University Press, Oxford, 2005.

[7] M. K. Gdoura, Problème de stokes avec des conditions aux limites nonlinèaires: analyse numèrique et algorithmes de rèsolution, Ph.D. thesis, Thèse en co-tutelle, Universitè Tunis El Manar et Universitè de Caen Basse Normandie (2011).

[8] G. H. Golub, C. F. V. Loan, Matrix Computation, The Johns Hopkins University Press: Baltimore, 1996.

[9] J. Haslinger, I. Hlaváček, J. Nečas, Numerical methods for unilateral problems in solid mechanics, Handbook of Numerical Analysis, Volume IV, Part 2, North Holland, Amsterdam 4 (1996) 313–485.

[10] J. Koko, Vectorized Matlab codes for the Stokes problem with P1-bubble/P1 finite element, url: `http://www.isima.fr/~jkoko/Codes.html` [online] (2012).

[11] R. Kučera, Convergence rate of an optimization algorithm for minimizing quadratic functions with separable convex constraints, SIAM Journal on Optimization 2 (19) (2008) 846–862.

[12] R. Kučera, J. Machalová, H. Netuka, P. Ženčák, An interior point algorithm for the minimization arising from 3d contact problems with friction, Optimization Methods and Software 6 (28) (2013) 1195–1217.

[13] J. Nocedal, A. Wächter, R. A. Waltz, Adaptive barrier strategies for nonlinear interior methods, TR RC 23563, IBM T.J. Watson Research Center.

[14] P.-O. Persson, G. Strang, A simple mesh generator in matlab, SIAM Review 46 (2005) 329–345.

[15] I. J. Rao, K. Rajagopal, The effect of the slip boundary condition on the flow of fluids in a channel, Acta Mechanica 135 (1999) 113–126.

[16] S. J. Wright, Primal-Dual Interior-Point Methods, SIAM, Philadelphia, 1997.